Lifetimes and transition probabilities for the low-lying states in ^{131}I and ^{132}Xe

S. S. Alam,[1,2] T. Bhattacharjee,[1,2,*] D. Banerjee,[3] A. Saha,[1,2] S. Das,[4] M. Saha Sarkar,[4] and S. Sarkar[5]

[1]*Variable Energy Cyclotron Centre, Kolkata 700 064, India*

[2]*Homi Bhabha National Institute, Training School Complex, Anushakti Nagar, Mumbai 400 094, India*

[3]*RCD-BARC, Variable Energy Cyclotron Centre, Kolkata 700 064, India*

[4]*Saha Institute of Nuclear Physics, Kolkata 700 064, India*

[5]*Indian Institute of Engineering Science and Technology, Shibpur, West Bengal 711 103, India*

(Received 13 August 2018; revised manuscript received 26 November 2018; published 8 January 2019)

Lifetimes are measured for the low-lying states of ^{131}I and ^{132}Xe nuclei populated from the decay of radio-chemically separated Te fission fragments. The VENTURE array comprised of eight fast $CeBr_3$ detectors is used for the lifetime measurement with γ-γ fast timing technique. Large basis shell model calculations have been performed with the "NUSHELLX" code to interpret the low-lying level structure and to calculate level lifetimes in ^{131}I and ^{132}Xe. The measured lifetimes and absolute transition probabilities are discussed in the light of systematics with the neighboring nuclei. Single particle excitation and loss of collectivity is observed with increasing neutron number up to $N = 82$, validating the double shell closure at ^{132}Sn. Enhanced $B(E1)$ and $B(E3)$ strengths are found for the 1646-keV, $11/2^-$ level in ^{131}I.

DOI: 10.1103/PhysRevC.99.014306

I. INTRODUCTION

The availability of spectroscopic information around ^{132}Sn is in striking contrast to the richness surrounding the classical doubly magic nuclei, viz., ^{16}O, ^{40}Ca, and ^{208}Pb. This is mainly because of the experimental difficulty in accessing this region by compound nuclear or transfer reactions using the available target-projectile combinations. Fission is one of the most accessed pathways by which these nuclei can be studied [1–4].

The validity of double shell closure near ^{132}Sn has been revealed by exploring the low-lying states of the nuclei having few proton (neutron) particles (holes) about $Z = 50$ and $N = 82$ [5–7]. More studies with complete spectroscopic information on the excited levels of these nuclei are, however, warranted to enrich the structure information in the poorly studied region around ^{132}Sn [8,9]. In particular, the measurement of electromagnetic transition probabilities are of specific importance as it can give direct understanding of the nucleon-nucleon interactions [5,10] and the evolution of collectivity around the $Z = 50$, $N = 82$ shell closure [11,12]. Existence of octupole correlation is known in the doubly closed ^{132}Sn [9], even-even Xe around $N = 82$ [13] and in other neutron deficient nuclei in this mass region [14,15] from the knowledge of $B(E1)$ and $B(E3)$ strengths. So, the lifetime measurements of the low-lying levels of the neutron rich iodine and xenon nuclei is of extreme importance in order to explore and enrich the nuclear structure around double shell closure at $Z = 50$ and $N = 82$ which is difficult to access experimentally.

In the present work, we focus on the lifetime measurement using the γ-γ fast timing technique for the low-lying levels of odd-A ^{131}I and even-even ^{132}Xe nuclei populated through the decay of radio-chemically separated Te fission fragments. The generalized centroid difference (GCD) method [16] has been used to analyze the experimental γ-γ time difference distribution obtained with the VENTURE array [17]. The large basis shell model (LBSM) calculations using the "NUSHELLX" code [18] have been performed to understand the excitation energies, dominant particle partitions, and level lifetimes for the low-lying levels in ^{131}I and ^{132}Xe. The transition strengths have been calculated from the measured level lifetime and discussed in the light of the systematics in the neighboring nuclei.

II. EXPERIMENTAL DETAILS

The excited states of ^{131}I and ^{132}Xe nuclei are populated as the β decay daughter and granddaughter of the respective Te fission fragments. The ^{131m}Te ($\tau \sim 33$ h) and ^{132}Te ($\tau \sim 3$ d) nuclei are produced with ^{nat}U(α, f) reaction with a 40-MeV α beam from the K-130 cyclotron at VECC, Kolkata. The ^{nat}U targets were prepared by using the electrodeposition technique on 25 μm-thick ^{nat}Al backing foils and multiple targets are irradiated with the help of the stacked foil irradiation technique. Irradiation was carried out for a duration of ∼48 h in order to have negligible relative yield of the short lived Te nuclei and the recoiling fission fragments are collected in ^{nat}Al catcher foils placed between two consecutive targets of the stack. The catcher foils are consequently treated for the radio-chemical separation of the active Te nuclei from rest of the fission fragments. The separated Te activity are kept in a liquid medium during the subsequent γ-γ coincidence measurements with the VENTURE [17] and VENUS [19] arrays. The VENTURE array with eight $1'' \times 1''$ fast $CeBr_3$ detectors has been used to

*Corresponding author: btumpa@vecc.gov.in

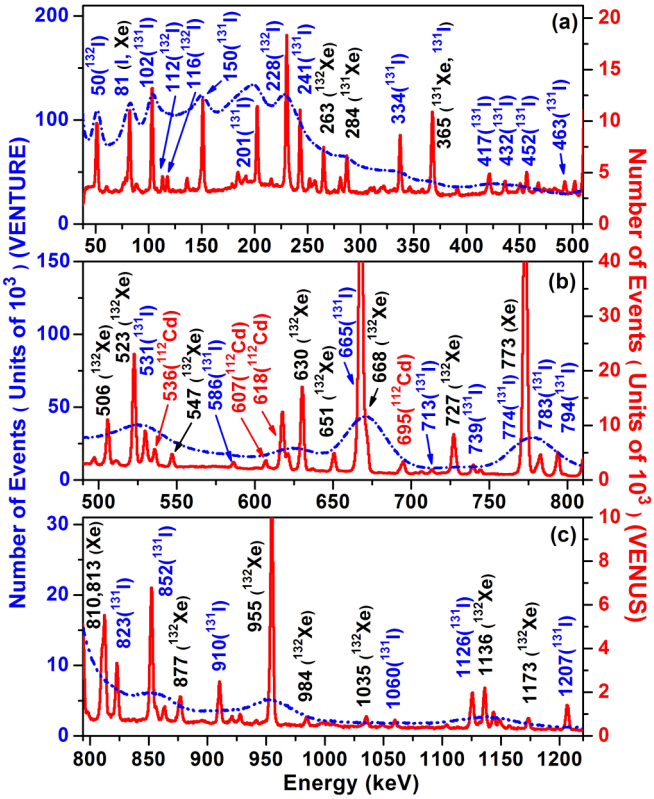

FIG. 1. The total projections (without any background subtraction) obtained from the $CeBr_3$ (blue dash dotted line) and clover detectors (red solid line) are shown from $CeBr_3$-$CeBr_3$ and $CeBr_3$-clover coincidences, respectively. The γ rays from different isotopes are identified and marked with different colours of text for I (blue), Xe (black), and Cd (red) (contamination).

detect the de-excited γ transitions for lifetime measurement and was set up along with the VENUS array of six Compton suppressed Clover HPGe detectors. The time resolution for a combination of two such $CeBr_3$ detectors is 154(8) ps at γ energy of ^{60}Co decay and is 188(3) ps for the array [17]. More details on the characteristics of the detectors and the arrays can also be found in Ref. [17] along with the details on the γ-γ fast timing analysis technique and the electronics setup used in the present work.

The GCD technique has been used for the analysis of γ-γ fast timing data in which a prompt response difference (PRD) curve is generated that represents the prompt time characteristics of the array. The prompt response depends on the PMT voltages, CFD settings, detector geometry, etc., along with other long-term effects. In the present work, The PRD curve shown in Fig. 19 of Ref. [17] has been used, as the data have been acquired with the same experimental setup and along with that reported for detailed description of the VENTURE characteristics presented in Ref. [17]. Also, the prompt response was checked time to time with source data in order to check for any major deviation. The details on the generation of the PRD curve for the VENTURE array and the determination of the PRD value for a particular γ-γ cascade can also be found in Ref. [17].

III. RESULTS

The $CeBr_3$ total projection from the $CeBr_3$-$CeBr_3$ coincidences is shown in Fig. 1 and is compared with the clover total projection from $CeBr_3$-Clover coincidence. These total projections are obtained without any subtraction of the underlying background. The spectrum from clover detectors depicts the clean separation of Te isotopes from the rest of the fission fragments with a little contamination from the Ag isotopes that gives rise to the γ lines from ^{112}Cd. The lifetimes measured in the present work are listed in Table I with some of the relevant information. The measured lifetimes are compared with earlier results, wherever available.

During the lifetime measurement using the GCD method, the delayed and antidelayed time distributions for different

TABLE I. Levels of ^{132}Xe and ^{131}I, for which lifetime measurements have been carried out in the present work. The lifetimes are calculated by using the equation $\tau = \frac{1}{2}(\Delta C_{FEP} - PRD)$. The quoted errors in lifetime are calculated by considering the standard deviation, i.e., $2\sigma \sim 7$ ps, obtained in the generation of PRD curve and the errors estimated for the ΔC values. The lifetimes marked with $\star$ has been considered for some systematic error as described in text. For the cases where the measured lifetimes are less than the estimated error, the upper limits of lifetimes are shown. The J^π values are taken as per the assignments shown in Table II.

Nucleus	E_x (keV)	J^π	Cascade (keV)	ΔC_{expt} (ps)	ΔC_{BG} (ps) (feeder)	p/b	ΔC_{BG} (ps) (decay)	p/b	t_{corr} (ps) (total)	ΔC_{FEP} (ps)	PRD (ps)	Lifetime (τ) (ps) Pres. work	Lit. [20–24]
^{131}I	774	$11/2_1^+$	1126–774	203(3)	211(3)	1.66(6)	164(1)	2.78(4)	5(2)	208(4)	165	22(5)	
	852	$9/2_1^+$	794–852	−10(4)	−22(8)	1.1(2)	5(2)	1.22(2)	−1(4)	−11(6)	−28	9(5)	
	1646	$11/2_1^-$	334–794	−228(2)	−267(5)	1.04(1)	−249(5)	1.86(3)	25(3)	−203(4)	−248	23(5)	
	1797	$15/2_1^-$	102–241									8.4(7) ns	8.5(3) ns
	1899	$13/2^-$	81–1126	−692(5)	−814(2)	1.14(1)	−784(14)	1.58(5)	83(6)	−609(8)	−676	34(6)	
^{132}Xe	668*	2_1^+	630–668	−14(2)	−21(3)	1.50(2)	−39(1)	2.68(3)	7(2)	−7(3)	−19	$\leqslant$8	6.1(5)–9.7(30)
	1298*	2_2^+	506–630	−48(2)	−42(2)	1.23(1)	−58(3)	1.60(2)	1(1)	−47(2)	−66	10(8)	4.4(4)
	1440	4_1^+	955–773	109(1)	102(4)	1.55(4)	95(3)	2.44(3)	6(2)	115(2)	87	14(5)	2.6(2)
	1963	4_2^+	877–523	186(4)	185(2)	1.04(2)	163(1)	1.30(1)	10(3)	196(5)	177	10(5)	

γ-γ cascades are analyzed to determine the experimental centroid difference ($\Delta C_{\rm expt}$). Appropriate background corrections, following similar methods as described in Ref. [25], are employed in the present work for determining the background corrected centroid differences for the full energy peak (FEP) ($\Delta C_{\rm FEP}$). The following sets of equations were used for the determination of $\Delta C_{\rm FEP}$s after accounting for the Compton background underlying both the FEPs (feeder and decay of a cascade) and to determine the level lifetimes with their errors:

$$\Delta C_{\rm FEP} = \Delta C_{\rm expt} + t_{\rm corr}$$

where

$$t_{\rm corr} = \frac{1}{2}[t_{\rm corr}({\rm feeder}) + t_{\rm corr}({\rm decay})],$$
$$t_{\rm corr}({\rm feeder}) = \left[\frac{\Delta C_{\rm expt} - \Delta C_{\rm BG}}{p/b}\right]_{\rm feeder},$$
$$t_{\rm corr}({\rm decay}) = \left[\frac{\Delta C_{\rm expt} - \Delta C_{\rm BG}}{p/b}\right]_{\rm decay}, \quad (1)$$
$$\tau = \frac{1}{2}[\Delta C_{\rm FEP} - {\rm PRD}],$$
$$\delta\tau = \frac{1}{2}\sqrt{(\delta\Delta C_{\rm expt})^2 + (\delta t_{\rm corr})^2 + (\delta{\rm PRD})^2}. \quad (2)$$

The $t_{\rm corr}$ represents the total background corrections that is necessary to be added to the centroid difference $\Delta C_{\rm expt}$, obtained from the γ-γ gating on the casade γ energies ($E_{\rm feeder}$ and $E_{\rm decay}$), and "p/b" represents the peak to background ratios. The $\Delta C_{\rm BG}$ values for feeder and decay γ rays were obtained by fitting the background pattern surrounding the energy of interest while taking the centroid differences corresponding to the coincidences among the photopeak of feeder (decay) and the Compton background neighboring to decay (feeder) γ rays in a particular cascade. The PRD is determined from the calibrated prompt time curve of the VENTURE array as described in Sec. II. Two standard deviations ($2\sigma \sim 7$ ps), obtained in the prompt time calibration, was considered while calculating the error in measured lifetime following Eq. (2).

Figures 2 and 3 demonstrate the above analysis procedure of lifetime measurement, considering two selective cascades of 630–688 keV of ^{132}Xe and 1126–774 keV of ^{131}I, respectively. In both of these figures, the gated projections from $CeBr_3$-$CeBr_3$ and $CeBr_3$-Clover coincidences are shown which are obtained by setting the $CeBr_3$ gate for (a) $E_{\rm feeder}$ and (b) $E_{\rm decay}$, respectively. The comparison of these two projections was helpful in selecting the energy gate for lifetime measurement and to identify if there is any unresolved photopeak around the energy of interest. Such peaks are marked with ⋆, if arising due to known γ-γ coincidences and with a # if it is due to coincidences with the Compton background underlying the gated photopeak. An extra systematic error has been added to the measured lifetime of the level in case the photopeak neighboring to the transition of interest was found to be disturbing the measurement and such levels are indicated by ⋆ in Table I. The background analysis is also demonstrated in Figs. 2 and 3, both around (c) $E_{\rm decay}$ and (d) $E_{\rm feeder}$, respectively. The background corrections are shown with respect to PRD = 0 at the reference energy value. The

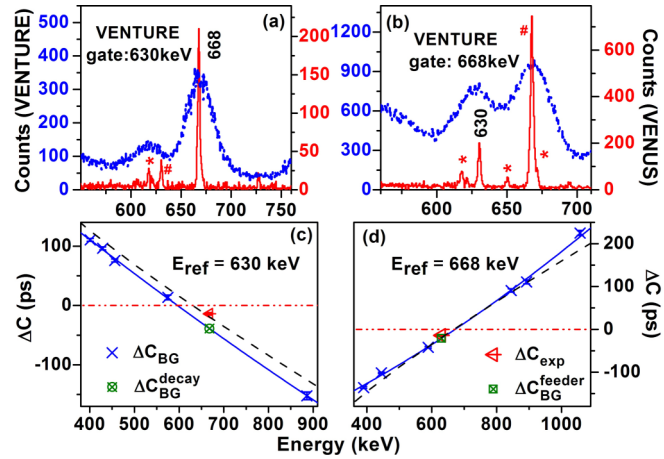

FIG. 2. The $CeBr_3$ energy gated projections of $CeBr_3$ (blue dash-dotted lines) and clover (red solid lines) detectors are shown with gate on (a) feeder (630 keV) and (b) decay (668 keV) γ rays of 630–668 keV cascade of ^{132}Xe. The photopeaks observed in (a) and (b) are marked with ⋆ and # respectively, in case they arise from known γ-γ coincidences or from the coincidence with the Compton background under the gating transition. The background analysis for this cascade are shown in panels (c) and (d) where $\Delta C_{\rm BG}$ values are shown with respect to PRD = 0 at $E_{\rm ref}$. The PRD curve is also shown with black dashed line by making PRD = 0 at $E_{\rm ref}$. The red dash-dotted line is drawn to guide the eye for ΔC or PRD = 0.

value of $\Delta C_{\rm expt}$ is also indicated on the figures and the same is taken from the separation between the delayed and antidelayed TAC projections shown in Fig. 4 for all the cascades listed in Table I. All kinds of centroid difference (ΔC) values obtained from this analysis and required for the determination of level lifetime are listed in Table I.

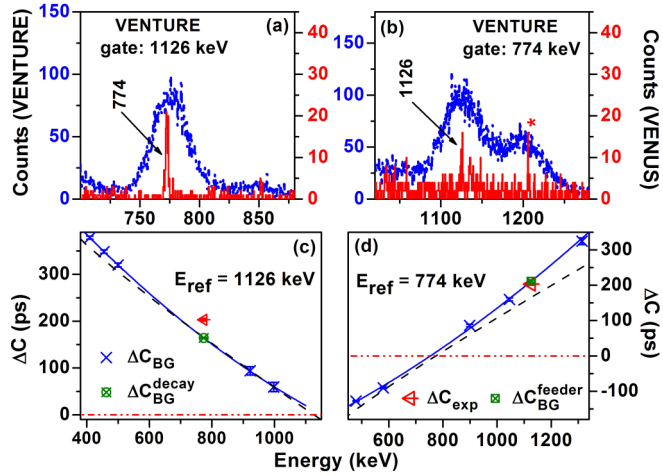

FIG. 3. The $CeBr_3$ energy gated projections of $CeBr_3$ (blue dash-dotted lines) and clover (red solid lines) detectors are shown with gate on (a) feeder (1126 keV) and (b) decay (774 keV) γ rays of 1126–774-keV cascade of ^{131}I. The background analysis for this cascade are shown in panels (c) and (d) where $\Delta C_{\rm BG}$ values are shown with respect to PRD = 0 at $E_{\rm ref}$. The PRD curve is also shown with black dashed line by making PRD = 0 at $E_{\rm ref}$. The red dash-dotted line is drawn to guide the eye for ΔC or PRD = 0.

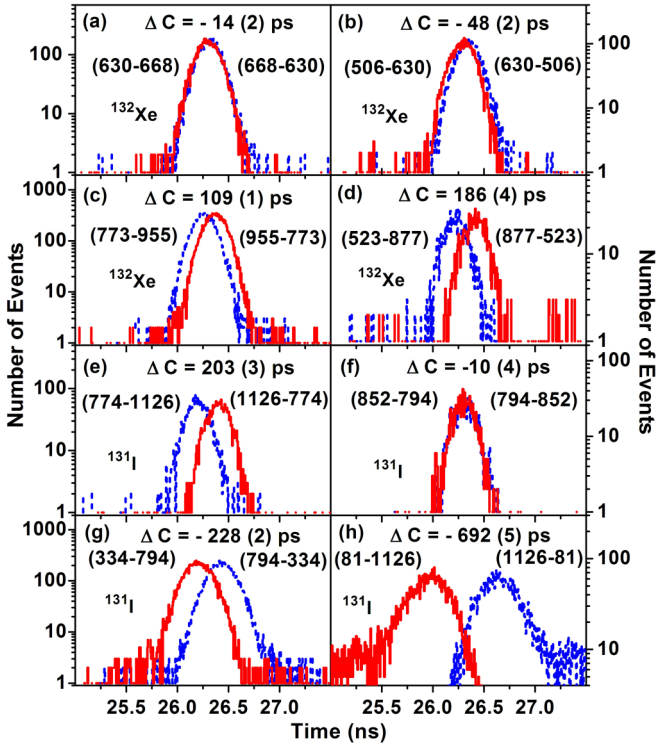

FIG. 4. The delayed and antidelayed TAC spectra for few cascades of ^{132}Xe (a)–(d) and ^{131}I (e)–(h) nuclei, used for the lifetime measurement with GCD method. The delayed and antidelayed time distributions are shown with red (solid) and blue (dotted) lines respectively.

The lifetimes measured with GCD method are shown in Table I in comparison to the earlier works, wherever available. Only the upper limit of lifetime is shown when the measured value is found to be less than the error obtained in the measurement. Prior to the present measurement, the level lifetimes for the 511.9 keV level of ^{106}Pd and the 160.6 and 383.8 keV levels of ^{133}Cs were reproduced from the same experimental setup, as described in Ref. [17]. In the present measurement, a systematic error was required to be added to the lifetimes of the levels marked with ⋆ in Table I. Among these, the 621 keV peak was found to be contaminating both the 630–668 (668 keV, 2_1^+ level of ^{132}Xe) and 506–630 (1298 keV, 2_2^+ level of ^{132}Xe) cascades. As the lifetime of the decaying and feeding levels of the 621 keV transition is not known, an error of 3 ps ($\sim 1\sigma$) was added to the lifetimes of these two levels. No contaminations were found, however, that can be considered as disturbing transitions for the remaining levels listed in Table I.

The present measurement could yield the lifetimes of the 774 keV ($11/2_1^+$), 852 keV ($9/2_1^+$), 1646 keV ($11/2_1^-$), and 1899 keV ($13/2_1^-$) levels of ^{131}I with the GCD method. None of these lifetimes are known in the literature and thus the present work provides these data for the first time. Along with ^{131}I, the lifetime measurement was also explored for the first few excited levels in ^{132}Xe which was yielded from the decay of ^{132}I. However, according to the data available for the Xe nuclei around $N = 82$ [26], the lifetimes for most of these

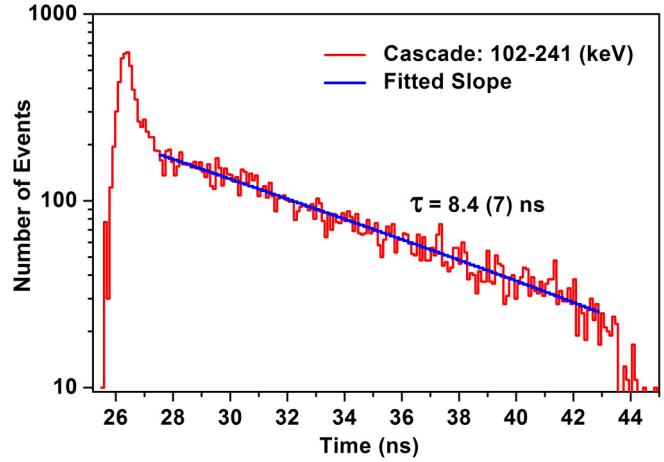

FIG. 5. The time distribution obtained for the 102–241 keV cascade with an appropriate background subtraction is shown.

levels in ^{132}Xe are expected to be below the standard deviation of the PRD. So, the precise determination of lifetimes for these levels in ^{132}Xe are difficult as the values are at the limits of the capability of the present experiment. Among these, the lifetime of the 2_1^+ level was measured, prior to the present work, with different techniques and the corresponding values vary among themselves between 6.1(5) and 9.7(30) ps [23,24]. Considering this variation for the 2_1^+ level, it is observed that the present measurement could reasonably reproduce the level lifetime of the first two excited levels in ^{132}Xe. In the case of the next excited level (4_1^+), however, the lifetime value yielded with the present GCD analysis is on the higher side in comparison to the earlier Coulomb excitation experiments [20,23,24]. In addition, the level lifetime for the 4_2^+ level in ^{132}Xe could also be measured for the first time in the present work. Along with the lifetime measurement with the GCD method, the lifetime of the 1797 keV ($15/2_1^-$) level of ^{131}I was also measured with the slope method. This was done by using the time distribution spectrum for the 102–241 keV cascade. The time distribution spectra and the slope fit for the 102–241 keV cascade is shown in Fig. 5 and the present measurement yielded a level lifetime of 8.4(7) ns which is in agreement with the earlier measurements [21] and listed in Table I.

The known experimental level sequences and the level lifetimes obtained for ^{131}I and ^{132}Xe have been interpreted from LBSM calculations performed with the NUSHELLX code as described in Sec. IV and the structure associated to different excited levels in these two nuclei is discussed in Sec. V.

IV. SHELL MODEL CALCULATION

In order to understand the structure of the low-lying states in ^{131}I and ^{132}Xe nuclei, LBSM calculations were performed using the code NUSHELLX [18]. The calculation considered ^{100}Sn as core and the particles were distributed over the 50–82 subshell space comprised of ($1g_{7/2}$, $2d_{5/2}$, $2d_{3/2}$, $3s_{1/2}$, $1h_{11/2}$) single particle orbitals. The calculations were carried out using proton-neutron formalism in full valence space without any truncation and using the $sn100pn$ interaction

[27], available with the code. The Hamiltonian consisted of four parts, treating the neutron-neutron, neutron-proton, proton-proton, and Coulomb repulsion between the protons. The residual two body matrix element of this interaction was obtained starting with a G matrix derived from the CD-Bonn nucleon-nucleon potential [28]. The single particle energies used in the calculation are 0.807 20 ($\pi 1g_{7/2}$), 1.562 30 ($\pi 2d_{5/2}$), 3.316 00 ($\pi 2d_{3/2}$), 3.223 80 ($\pi 3s_{1/2}$), 3.605 10 ($\pi 1h_{11/2}$), −10.608 90 ($\nu 1g_{7/2}$), −10.289 30 ($\nu 2d_{5/2}$), −8.716 70 ($\nu 2d_{3/2}$), −8.694 40 ($\nu 3s_{1/2}$), and −8.815 20 ($\nu 1h_{11/2}$) MeV respectively. In Table II, the calculated excitation energies are compared with the experimental energies of the low-lying levels, mostly below 2.0 MeV, in the iodine and xenon nuclei under study.

The decomposition of angular momentum of proton and neutron ($I_\pi \otimes I_\nu$) for each level is listed in Table II along with the dominant particle partitions contributing to the configuration mixed (J^π) states. Only those I_π-I_ν combinations are listed which have a contribution of greater than 10% in the total wave function. Different partitions obtained for a particular coupling are also listed in the table. In general, all those partitions having probability >5% are listed, wherever available. However, there are some cases where all the partitions are of less than 5% strength and in such a situation the partition having the maximum probability is only listed. It is important to mention that the corresponding partitions listed in the table, however, account for not more than 25% of the total partitions involved in constituting the state. This indicates a tremendous fragmentation of the wave functions, i.e., configuration mixing, in almost all the levels in ^{131}I and ^{132}Xe.

The transition probabilities, corresponding to the decay of excited levels in ^{131}I and ^{132}Xe, have been calculated using effective charges ($e^p = 1.35$, $e^n = 0.35$) and g factors ($g_l^p = 1.0$, $g_s^p = 5.586$, $g_l^n = 0.0$ and $g_s^n = -3.826$). The lifetimes have been calculated from these transition probabilities by considering the theoretical branching and experimental γ energy values. The conversion coefficient for a particular transition was calculated from the BrIcc code [29]. The lifetime values obtained from the calculation have been compared with the experimental results for the positive parity levels, as shown in Table II. The lifetimes of all the positive parity levels in ^{131}I and ^{132}Xe are reasonably reproduced from the calculation. However, using the above method, the level lifetimes could not be directly estimated for the negative parity levels of ^{131}I, viz., 1646 keV ($11/2_1^-$), 1797 keV ($15/2_1^-$), and 1899 keV ($13/2_1^-$). These levels are known to de-excite by strong $E1$ decays and the single particle orbitals available in the chosen model space of our calculation do not allow such $E1$ decay to occur. However, the lifetime for two of these levels could be calculated from partial lifetimes obtained from shell model calculation and using the experimental branching ratios. These calculations are discussed below in Sec. V and the lifetime values are tabulated in Table II.

V. DISCUSSION

The level structures for the ^{131}I and ^{132}Xe nuclei are discussed below based on the results of shell model calculations given above and comparison with systematics of the neighboring nuclei. The systematic comparison has been helpful in understanding the evolution of level structure in these nuclei as a function of neutron number. This has been done by comparing the level energies and the transition rates for individual levels. The reduced transition probabilities [$B(E\lambda)$] have been estimated, using the standard formulations [30], from the measured level lifetimes and the known branching and mixing ratios [21,22].

A. ^{131}I

The level energies of ^{131}I up to 2.0 MeV could be well reproduced from present shell model calculation. However, in Table II, only the low-lying levels up to 1060 keV and a few higher lying levels relevant to the present measurements and discussions are shown. Both of the second and third excited levels in ^{131}I at 493 and 602 keV have experimental J^π assignment of $3/2^+$ or $5/2^+$ [21]. The present calculation shows two such levels at 450 and 653 keV excitations which have J^π values of $5/2^+$ and $3/2^+$, respectively, and could be assigned accordingly. This is, however, contrary to the earlier shell model work of Ref. [31] and the experimental level sequences in ^{127}I and ^{129}I, where the first $3/2^+$ level is below the second $5/2^+$. The 774 keV level has been known to have the J^π assignment of $9/2^+$ or $11/2^+$ [21]. The present calculation predicts one $11/2^+$ level at 803 keV and accordingly the 774 keV level is suggested to have a $11/2^+$ assignment. The next four excited levels at 852, 876, 1006, and 1060 keV are also well reproduced in the present calculation. The 1006-keV level possibly has $7/2^+$ assignment as 1040 keV ($7/2^+$) is the only level that was produced from the present calculation between 896 ($1/2^+$) and 1169 ($9/2^+$) keV. The next two levels, shown in Table II, at 1556 and 1596 keV are predicted at 1554 and 1649 keV from the present calculation. Our calculation could also reproduce all the negative parity levels up to 1925 keV ($11/2^-$) in ^{131}I. The J^π values of both the 1797 and 1899 keV levels were assigned to have ($9/2^-$, $11/2^-$, $13/2^-$) in the NNDC database [21]. However, the angular correlation and nuclear orientation experiments [32] suggested the spin parity of $15/2^-$ and $13/2^-$, respectively, for the 1797 and 1899 keV levels. The said assignment of the 1797 keV level is also supported by the recent experimental observation from multinucleon transfer with ^{136}Xe [33] and the $M1$ nature of the 102 keV transition connecting the 1899 and 1797 keV levels. In our present calculation, two negative parity levels of $15/2^-$ and $13/2^-$ are predicted at 1776 and 1841 keV, respectively, and are accordingly associated with the 1797 and 1899 keV levels. The recent experiment [33] on ^{131}I also supports the spin assignments of the 1556 and 1596 keV levels as $15/2^+$ and $13/2^+$, respectively. The excitation energies for a few other levels observed in this multinucleon transfer experiment, viz., 1881 keV ($15/2^+$), 1885 keV ($17/2^-$), and 1918 keV ($19/2^-$), are also reproduced from the present work at 1832, 2011, and 1956 keV, respectively, but are not listed in Table II.

As mentioned in Sec. IV, a strong fragmentation of configuration was found for the excited levels in ^{131}I and <1% strength was found for 35–55% of the total partitions. Such

TABLE II. The excitation energy, most dominant particle partitions, and level lifetimes for the low-lying levels in ^{132}Xe and ^{131}I, obtained from shell model calculation with NUSHELLX, are shown. The experimental values are also shown for comparison. (a) shows the % probability of coupling between a particular combination of I_π and I_ν. (b) represents the % probability of a specific partition for a particular coupling.

Nucleus	E_x (keV)		J^π		I_π	I_ν	% prob. (a)	Major partition	% prob. (b)	Lifetime (ps) (pres. work)	
	expt.	calc.	expt.	calc.						expt.	calc.
^{132}Xe	0	0	0^+	0^+	0^+	0^+	66.70	$\pi(1g^4_{7/2}) \otimes \nu(2d^{-2}_{3/2}1h^{-2}_{11/2})$	11.04		
								$\pi(1g^2_{7/2}2d^2_{5/2}) \otimes \nu(2d^{-2}_{3/2}1h^{-2}_{11/2})$	6.07		
					2^+	2^+	29.06	$\pi(1g^4_{7/2}) \otimes \nu(2d^{-2}_{3/2}1h^{-2}_{11/2})$	3.23		
	668	740	2^+	2^+	0^+	2^+	42.91	$\pi(1g^4_{7/2}) \otimes \nu(2d^{-2}_{3/2}1h^{-2}_{11/2})$	6.49	$\leqslant 8$	15
					2^+	0^+	31.40	$\pi(1g^4_7/2) \otimes \nu(2d^{-2}_{3/2}1h^{-2}_{11/2})$	4.82		
	1298	1413	2^+	2^+	0^+	2^+	39.22	$\pi(1g^4_{7/2}) \otimes \nu(2d^{-1}_{3/2}3s^{-1}_{1/2}1h^{-2}_{11/2})$	5.33	10(8)	11
								$\pi(1g^4_{7/2}) \otimes \nu(2d^{-2}_{3/2}1h^{-2}_{11/2})$	5.00		
					2^+	2^+	29.48	$\pi(1g^4_{7/2}) \otimes \nu(2d^{-2}_{3/2}1h^{-2}_{11/2})$	3.78		
					2^+	3^+	10.16	$\pi(1g^4_{7/2}) \otimes \nu(2d^{-1}_{3/2}3s^{-1}_{1/2}1h^{-2}_{11/2})$	1.50		
	1440	1525	4^+	4^+	0^+	4^+	22.99	$\pi(1g^4_{7/2}) \otimes \nu(2d^{-2}_{3/2}1h^{-2}_{11/2})$	3.66	14(5)	5
					2^+	2^+	33.15	$\pi(1g^4_{7/2}) \otimes \nu(2d^{-2}_{3/2}1h^{-2}_{11/2})$	4.77		
					4^+	0^+	21.03	$\pi(1g^4_{7/2}) \otimes \nu(2d^{-2}_{3/2}1h^{-2}_{11/2})$	2.99		
	1803	1922	3^+	3^+	0^+	3^+	37.13	$\pi(1g^4_{7/2}) \otimes \nu(2d^{-1}_{3/2}3s^{-1}_{1/2}1h^{-2}_{11/2})$	6.83		
					2^+	2^+	32.36	$\pi(1g^4_{7/2}) \otimes \nu(2d^{-1}_{3/2}3s^{-1}_{1/2}1h^{-2}_{11/2})$	3.12		
					2^+	4^+	10.88	$\pi(1g^4_{7/2}) \otimes \nu(2d^{-1}_{3/2}3s^{-1}_{1/2}1h^{-2}_{11/2})$	1.15		
	1850	1697	0^+ & 2^+	0^+	0^+	0^+	57.02	$\pi(1g^4_{7/2}) \otimes \nu(2d^{-1}_{3/2}3s^{-2}_{1/2})$	8.84		
								$\pi(1g^2_{7/2}2d^2_{5/2}) \otimes \nu(2d^{-2}_{3/2}1h^{-2}_{11/2})$	6.41		
					2^+	2^+	36.84	$\pi(1g^2_{7/2}2d^2_{5/2}) \otimes \nu(2d^{-2}_{3/2}1h^{-2}_{11/2})$	3.50		
	1963	1887	4^+	4^+	0^+	4^+	16.43	$\pi(1g^4_{7/2}) \otimes \nu(2d^{-2}_{3/2}1h^{-2}_{11/2})$	3.49	10(5)	1
					4^+	0^+	46.47	$\pi(1g^4_{7/2}) \otimes \nu(2d^{-2}_{3/2}1h^{-2}_{11/2})$	7.64		
	1986	1881	2^+	2^+	0^+	2^+	17.22	$\pi(1g^4_{7/2}) \otimes \nu(2d^{-2}_{3/2}1h^{-2}_{11/2})$	4.09		
					2^+	0^+	34.50	$\pi(1g^2_{7/2}2d^2_{5/2}) \otimes \nu(2d^{-2}_{3/2}1h^{-2}_{11/2})$	4.15		
					2^+	2^+	11.15	$\pi(1g^4_{7/2}) \otimes \nu(2d^{-1}_{3/2}3s^{-1}_{1/2}1h^{-2}_{11/2})$	1.19		
					4^+	2^+	20.72	$\pi(1g^2_{7/2}2d^2_{5/2}) \otimes \nu(2d^{-2}_{3/2}1h^{-2}_{11/2})$	1.71		
	2112	1976	6^+	6^+	4^+	2^+	11.64	$\pi(1g^2_{7/2}2d^1_{5/2}) \otimes \nu(2d^{-2}_{3/2}1h^{-2}_{11/2})$	1.57		
					6^+	0^+	53.17	$\pi(1g^3_{7/2}2d^1_{5/2}) \otimes \nu(3s^{-2}_{1/2}1h^{-2}_{11/2})$	5.10		
								$\pi(1g^3_{7/2}2d^1_{5/2}) \otimes \nu(2d^{-2}_{3/2}1h^{-2}_{11/2})$	14.62		
					6^+	2^+	10.31	$\pi(1g^3_{7/2}2d^1_{5/2}) \otimes \nu(2d^{-2}_{3/2}1h^{-2}_{11/2})$	2.56		
^{131}I	0	0	$7/2^+$	$7/2^+$	$5/2^+$	2^+	10.02	$\pi(1g^3_{7/2}) \otimes \nu(2d^{-2}_{3/2}1h^{-2}_{11/2})$	2.28		
					$7/2^+$	0^+	68.33	$\pi(1g^3_{7/2}) \otimes \nu(3s^{-2}_{1/2}1h^{-2}_{11/2})$	5.92		
								$\pi(1g37/2) \otimes \nu(2d^{-2}_{3/2}1h^{-2}_{11/2})$	18.66		
	150	246	$5/2^+$	$5/2^+$	$5/2^+$	0^+	51.26	$\pi(1g^3_{7/2}) \otimes \nu(2d^{-2}_{3/2}1h^{-2}_{11/2})$	10.46		
								$\pi(1g^2_{7/2}2d^1_{5/2}) \otimes \nu(2d^{-2}_{3/2}1h^{-2}_{11/2})$	6.29		
					$5/2^+$	2^+	11.95	$\pi(1g^3_{7/2}) \otimes \nu(2d^{-1}_{3/2}3s^{-1}_{1/2}1h^{-2}_{11/2})$	1.52		
					$7/2^+$	2^+	24.74	$\pi(1g^3_{7/2}) \otimes \nu(2d^{-2}_{3/2}1h^{-2}_{11/2})$	5.38		
	493	450	$3/2^+$,$5/2^+$	$5/2^+$	$5/2^+$	0^+	58.24	$\pi(1g^2_{7/2}2d^1_{5/2}) \otimes \nu(2d^{-2}_{3/2}1h^{-2}_{11/2})$	12.94		
					$5/2^+$	2^+	13.64	$\pi(1g^2_{7/2}2d^1_{5/2}) \otimes \nu(2d^{-2}_{3/2}1h^{-2}_{11/2})$	2.91		
					$7/2^+$	2^+	12.33	$\pi(1g^3_{7/2}) \otimes \nu(2d^{-2}_{3/2}1h^{-2}_{11/2})$	2.18		
	602	653	$3/2^+$,$5/2^+$	$3/2^+$	$3/2^+$	0^+	42.53	$\pi(1g^3_{7/2}) \otimes \nu(2d^{-2}_{3/2}1h^{-2}_{11/2})$	11.00		

TABLE II. *(Continued.)*

Nucleus	E_x (keV)		J^π		I_π	I_ν	% prob. (a)	Major partition	% prob. (b)	Lifetime (ps) (pres. work)	
	expt.	calc.	expt.	calc.						expt.	calc.
					$5/2^+$	2^+	15.15	$\pi(1g_{7/2}^3)\otimes\nu(2d_{3/2}^{-2}1h_{11/2}^{-2})$	4.66		
					$7/2^+$	2^+	29.68	$\pi(1g_{7/2}^3)\otimes\nu(2d_{3/2}^{-2}1h_{11/2}^{-2})$	8.90		
	774	803	$9/2^+$,$11/2^+$	$11/2^+$	$7/2^+$	2^+	44.33	$\pi(1g_{7/2}^3)\otimes\nu(2d_{3/2}^{-2}1h_{11/2}^{-2})$	12.71	22(5)	11
					$11/2^+$	0^+	32.36	$\pi(1g_{7/2}^3)\otimes\nu(2d_{3/2}^{-2}1h_{11/2}^{-2})$	10.18		
	852	872	$9/2^+$	$9/2^+$	$7/2^+$	2^+	49.46	$\pi(1g_{7/2}^3)\otimes\nu(2d_{3/2}^{-1}3s_{1/2}^{-1}1h_{11/2}^{-2})$	9.02	9(5)	4
								$\pi(1g_{7/2}^3)\otimes\nu(2d_{3/2}^{-2}1h_{11/2}^{-2})$	9.36		
					$9/2^+$	0^+	22.34	$\pi(1g_{7/2}^3)\otimes\nu(2d_{3/2}^{-2}1h_{11/2}^{-2})$	6.15		
	876	896	$1/2^+$	$1/2^+$	$1/2^+$	0^+	42.51	$\pi(1g_{7/2}^2 3s_{1/2}^1)\otimes\nu(2d_{3/2}^{-2}1h_{11/2}^{-2})$	9.41		
					$5/2^+$	2^+	43.14	$\pi(1g_{7/2}^2 2d_{5/2}^1)\otimes\nu(2d_{3/2}^{-2}1h_{11/2}^{-2})$	13.49		
	1006	1040		$7/2^+$	$5/2^+$	2^+	38.72	$\pi(1g_{7/2}^2 2d_{5/2}^1)\otimes\nu(2d_{3/2}^{-1}3s_{1/2}^{-1}1h_{11/2}^{-2})$	8.52		
								$\pi(1g_{7/2}^2 2d_{5/2}^1)\otimes\nu(2d_{5/2}^{-1}3s_{1/2}^{-1}1h_{11/2}^{-2})$	7.85		
					$7/2^+$	0^+	35.38	$\pi(1g_{7/2}^2 2d_{7/2}^1)\otimes\nu(2d_{3/2}^{-2}1h_{11/2}^{-2})$	10.9		
	1060	1169	$9/2^{(+)}$	$9/2^+$	$5/2^+$	2^+	33.56	$\pi(1g_{7/2}^2 2d_{5/2}^1)\otimes\nu(2d_{3/2}^{-2}1h_{11/2}^{-2})$	10.09		
					$9/2^+$	0^+	34.07	$\pi(1g_{7/2}^2 2d_{5/2}^1)\otimes\nu(2d_{3/2}^{-2}1h_{11/2}^{-2})$	10.31		
	1556	1554	+	$15/2^+$	$7/2^+$	4^+	16.96	$\pi(1g_{7/2}^3)\otimes\nu(2d_{3/2}^{-2}1h_{11/2}^{-2})$	5.25		
					$11/2^+$	2^+	29.89	$\pi(1g_{7/2}^3)\otimes\nu(2d_{3/2}^{-2}1h_{11/2}^{-2})$	9.70		
					$15/2^+$	0^+	32.98	$\pi(1g_{7/2}^3)\otimes\nu(2d_{3/2}^{-2}1h_{11/2}^{-2})$	9.96		
	1596	1649	+	$13/2^+$	$9/2^+$	2^+	21.93	$\pi(1g_{7/2}^2 2d_{5/2}^1)\otimes\nu(2d_{3/2}^{-2}1h_{11/2}^{-2})$	5.29		
					$13/2^+$	0^+	44.81	$\pi(1g_{7/2}^2 2d_{5/2}^1)\otimes\nu(2d_{3/2}^{-2}1h_{11/2}^{-2})$	13.58		
	1646	1606	$11/2^-$	$11/2^-$	$11/2^-$	0^+	56.72	$\pi(1g_{7/2}^2 1h_{11/2}^1)\otimes\nu(3s_{1/2}^{-2}1h_{11/2}^{-2})$	6.74	23(5)	
								$\pi(1g_{7/2}^2 1h_{11/2}^1)\otimes\nu(2d_{3/2}^{-2}1h_{11/2}^{-2})$	18.32		
					$11/2^-$	2^+	27.81	$\pi(1g_{7/2}^2 1h_{11/2}^1)\otimes\nu(2d_{3/2}^{-1}3s_{1/2}^{-1}1h_{11/2}^{-2})$	5.12		
								$\pi(1g_{7/2}^2 1h_{11/2}^1)\otimes\nu(2d_{3/2}^{-2}1h_{11/2}^{-2})$	5.94		
	1797	1776	$9/2^-$,$11/2^-$,$13/2^-$	$15/2^-$	$5/2^+$	5^-	13.02	$\pi(1g_{7/2}^3)\otimes\nu(2d_{3/2}^{-2}3s_{1/2}^{-1}1h_{11/2}^{-1})$	4.68	8.4(7) ns	22 ns
					$5/2^+$	7^-	10.02	$\pi(1g_{7/2}^3)\otimes\nu(2d_{3/2}^{-1}3s_{1/2}^{-2}1h_{11/2}^{-1})$	2.58		
					$7/2^+$	5^-	57.91	$\pi(1g_{7/2}^3)\otimes\nu(2d_{3/2}^{-2}3s_{1/2}^{-1}1h_{11/2}^{-1})$	21.25		
								$\pi(1g_{7/2}^3)\otimes\nu(2d_{3/2}^{-3}1h_{11/2}^{-1})$	8.27		
	1899	1841	$9/2^-$,$11/2^-$,$13/2^-$	$13/2^-$	$5/2^+$	5^-	14.42	$\pi(1g_{7/2}^3)\otimes\nu(2d_{3/2}^{-2}3s_{1/2}^{-1}1h_{11/2}^{-1})$	5.88	34(6)	44
					$7/2^+$	5^-	42.33	$\pi(1g_{7/2}^3)\otimes\nu(2d_{3/2}^{-2}3s_{1/2}^{-1}1h_{11/2}^{-1})$	15.21		
								$\pi(1g_{7/2}^3)\otimes\nu(2d_{3/2}^{-3}1h_{11/2}^{-1})$	6.17		
	1925	1916	$11/2^-$	$11/2^-$	$5/2^+$	5^-	17.28	$\pi(1g_{7/2}^3)\otimes\nu(2d_{3/2}^{-2}3s_{1/2}^{-1}1h_{11/2}^{-1})$	6.42		
					$7/2^+$	5^-	42.36	$\pi(1g_{7/2}^3)\otimes\nu(2d_{3/2}^{-2}3s_{1/2}^{-1}1h_{11/2}^{-1})$	15.07		
								$\pi(1g_{7/2}^3)\otimes\nu(2d_{3/2}^{-3}1h_{11/2}^{-1})$	6.17		

strong fragmentation of configuration conjectures the collective nature for these levels in ^{131}I. Considering the major configurations, the structure of the positive parity levels in this nucleus was found to be dominated by $\pi g_{7/2}$, $\nu h_{11/2}$, and $\nu d_{3/2}$ orbitals. The $5/2^+$ levels in ^{131}I have mixed configurations involving both $\pi g_{7/2}$ and $\pi d_{5/2}$ orbitals. This is not in line with much of the earlier understanding regarding the pure $\pi d_{5/2}$ configuration of the first excited state in ^{131}I [34,35]. The negative parity levels in ^{131}I was found to be developed from multiquasiparticle excitation involving both a $\pi h_{11/2}^1$ particle and a $\nu h_{11/2}^{-1}$ hole. From the present calculation, it was found that the lowest negative parity level at 1646 keV, $11/2^-$ has major contribution from the $\pi h_{11/2}^1$ particle in comparison

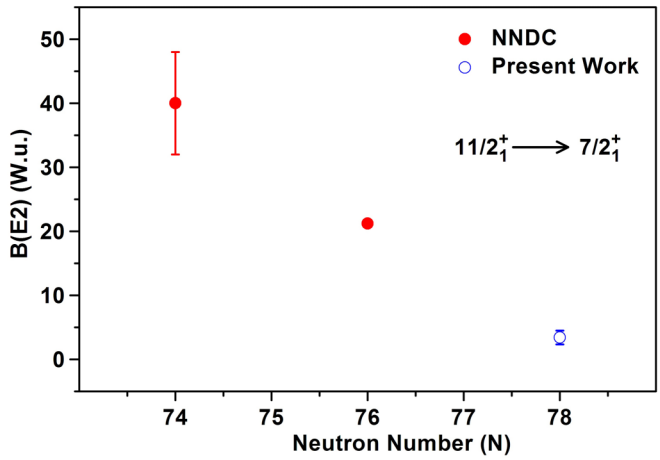

FIG. 6. The $B(E2)$ values for the decay of 774 keV, $11/2^+$ level in ^{131}I in comparison to that in neighboring nuclei is shown. The filled circles (red) represents the values calculated from the level lifetimes taken from NNDC database [26] and the open circle (blue) is for ^{131}I and is measured in the present work. The branching and mixing ratios are taken from NNDC database.

to the other higher lying negative parity levels in ^{131}I, viz., 1797, 1899, and 1925 keV, where both protons and neutrons were found to be contributing in the major partitions.

Among the two positive parity levels in ^{131}I for which lifetime measurement has been done in the present work, the 774 keV, $11/2^+$ level decays mainly by a strong $E2$ transition to the $7/2^+$ ground state, indicating a collective nature for this level. The $B(E2)$ value for the decay of the lowest $11/2^+$ levels in ^{131}I and its neighboring nuclei up to the $N = 82$ shell closure is shown in Fig. 6. The $B(E2)$ value for $11/2_1{}^+ \rightarrow 7/2_1{}^+$ decay shows a decreasing trend as a function of neutron number supporting the loss of collectivity as one approaches the double shell closure of ^{132}Sn.

As discussed in Sec. IV, the $E1$ decays from the negative parity levels in ^{131}I could not be calculated in the chosen shell model valence space. The lifetime of the 1797-keV $(15/2^-)$ level in ^{131}I was known from earlier works [35] and is also measured in the present work (cf. Table I) as 8.4(7) ns. This level mainly decays by the 201 and 241 keV transitions, which are known to be of $E1$ nature from the conversion electron measurement [36], and by considering these strong decays, no theoretical estimate of level lifetime was possible for this level. One 151 keV transition of very weak intensity is known from this level to the 1646 keV, $11/2^-$ level. Considering $E2$ multipolarity for this transition and by correcting for the branching ratios as available in NNDC [21], the lifetime for this level comes out to be 21 ns from the shell model calculation. The 1899 keV $(13/2_1^-)$ level decays by two strong transitions, viz. 102 keV ($M1$) and 1126 keV ($E1$). The measured lifetime of this level comes out to be 34(6) ps (cf. Table I). The present calculation estimates a lifetime of 116 ps for the 1899 keV level by considering only the 102 keV $M1$ decay. Considering this partial lifetime and the known branching of the 102 keV, the level lifetime of the 1899 keV level is estimated to be 44 ps which is close to the present measurement. The level lifetime of the 1646 keV, $11/2^-$ level was also measured for the first time in the present work (cf. Table I). However, no theoretical estimate could be made for this lifetime as the level is de-excited by two $E1$ transitions, viz., 586 and 794 keV, which carry the major share of decay out intensity and the nature of the other weak decays from this level are not available in the literature. The $E1$ decays from these negative parity levels are discussed in comparison to the systematics observed in the neighboring nuclei.

The 1646 keV, $11/2^-$ level decays by the 794 keV $E1$ transition to the 852 keV, $9/2^+$ level. The presence of $\Delta J = 1$, $\Delta\pi = -1$ proton orbitals ($\pi h_{11/2}$, $\pi g_{9/2}$) are necessary in the configuration of the initial (1646 keV, $11/2^-$) and the final (852 keV, $9/2^+$) levels for this $E1$ decay to occur. However, the major configurations for the 852 keV level were found to involve $\pi g_{7/2}^3$ protons and to have the same neutron hole configuration as that of 1646 keV level. Also, the excitation energy of the 852 keV level was very well reproduced from the present calculation with such a configuration. Hence, the origin of $E1$ decay from the 1646 keV level could not be explained from the present shell model calculation. In order to understand this, the decays of such $11/2^-$ levels observed in the neighboring iodine nuclei have been studied and are shown in Fig. 7. It is found that, in all these nuclei, the $E1$ decays are observed from the $11/2^-$ $(\pi h_{11/2}^1)$ level to the $9/2^+$ levels having configurations involving either $\pi d_{5/2}^1$ or $\pi g_{7/2}^1$. Also, no connection was found between these $11/2^-$ $(\pi h_{11/2}^1)$ levels to the proposed $\pi g_{9/2}^{-1}$ levels, wherever known. In addition, the excitation energy of the lowest $\pi g_{9/2}^{-1}$ level, known in these nuclei, was found to increase as a function of neutron number; and at $N = 74$, it was observed at a higher excitation compared to the $11/2^-$ $(\pi h_{11/2}^1)$ level. So, it may

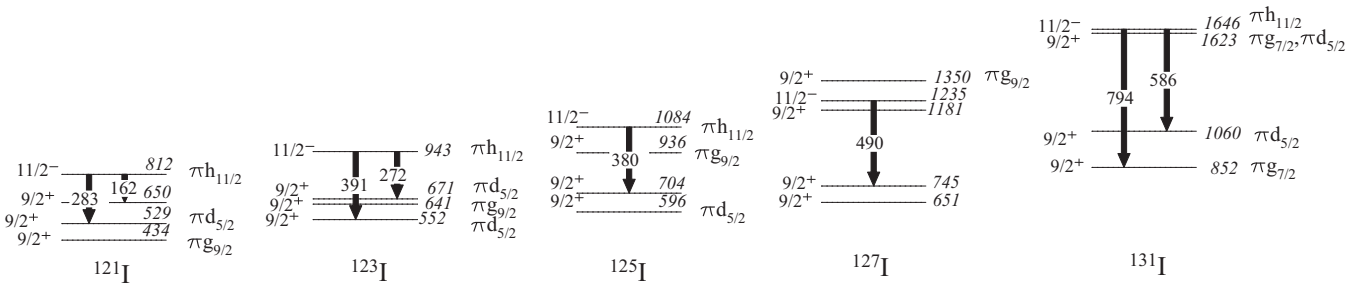

FIG. 7. The systematics of $E1$ decays from the $11/2^-$ levels in the iodine nuclei around ^{132}Sn.

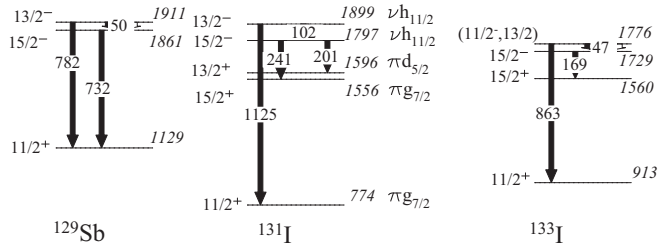

FIG. 8. The systematics of $E1$ decays from the $13/2^-$ and $15/2^-$ levels in the I and Sb nuclei around ^{132}Sn.

be conjectured that $\pi g_{9/2}^{-1}$ excitation in ^{131}I will be at higher excitation compared to the 1646 keV, $11/2^-$ level.

Both of the next two negative parity levels in ^{131}I, viz., 1797 keV $(15/2^-)$ and 1899 keV $(13/2^-)$, were found to have the involvement of the $\nu h_{11/2}$ hole in the major configurations obtained from the present shell model calculation. As discussed above for 1646-keV level, the strong $E1$ decays from these levels, viz. (1) 1797 keV $(15/2^-) \rightarrow$ 1556 keV $(15/2^+)$, (ii) 1797 keV $(15/2^-) \rightarrow$ 1596 keV $(13/2^+)$, and (iii) 1899 keV $(13/2^-) \rightarrow$ 773 keV $(11/2^+)$, could be explained only if a $\nu g_{9/2}^{-1}$ configuration is involved in the configuration of the final levels, viz., 774, 1556, and 1596 keV. However, all these three levels could be well reproduced in the present calculation with the involvement of $\nu d_{3/2}^{-2} h_{11/2}^{-2}$ configurations and without any contribution from $\nu g_{9/2}$. A systematic comparison of the $15/2^-$ and $13/2^-$ levels and their $E1$ decays neighboring to ^{131}I have also been shown in Fig. 8 where it is observed that these negative parity levels in ^{129}Sb and ^{133}I also show similar decays as observed in the case of ^{131}I. However, neither the configurations of these levels in ^{129}Sb and ^{133}I are known nor the existence of any $\nu g_{9/2}^{-1}$ configuration is yet found in these nuclei. Such neutron core excitation is, however, supposed to involve much higher excitation as predicted in ^{133}Cs [37].

Earlier, the possibility of an octupole excitation of the core, coupled to a single-quasiparticle state, was considered for the excitation of the 1797 keV level in ^{131}I (cf. Ref. [36]). In order to test such a conjecture, the $B(E1)$ and $B(E3)$ strengths obtained from the measured lifetimes are tabulated in Table III for the decay of the negative parity levels in ^{131}I. The $B(E3)$ rate calculated from the present shell model calculation is also shown in the table for comparison.

The $B(E1)$ rates from the 1646 keV $(11/2^-)$ level to the 852 and 1060 keV $(9/2^+)$ levels are found to be similar to that observed for the 3^- level in ^{114}Xe [38] where octupole collectivity has been established. It is, however, observed that the $B(E1)$ strengths from the 1797 and 1899 keV levels are not enhanced similar to the 1646 keV level. Moreover, by considering the pure $E3$ nature for the 1496 keV γ ray [1646 keV $(11/2^-) \rightarrow$ 150 keV $(5/2^+)$], the limit for the corresponding $B(E3)$ strength was estimated. This $B(E3)$ strength was observed to be <14 W.u. which is similar to that known for ^{132}Sn [9], $^{124-134}$Xe [13], $^{132-138}$Ba [39], and in other nuclei [40] in this mass region where octupole correlation has been observed. The octupole correlation around $Z = 56$ [41] is expected from the interaction of the two $\Delta J = 3$ orbitals, viz., $d_{5/2}$ and $h_{11/2}$, in 50–82 subshell space. The experimental $B(E3)$ value for the 1646 keV level was also reasonably reproduced from the present shell model calculation as evident from Table III. It comes out to be 5.5 and 11.0 W.u., by considering the effective proton charge (e^p) as 2.0 (cf. Refs. [10,42]) and 3.0, respectively. Most importantly, it was found that the $B(E3)$ value for this level, which was dominated by $\pi h_{11/2}$ configuration, is almost independent of the value of the effective neutron charge (e^n). On the contrary, the calculated $B(E3)$ value for the second $11/2^-$ level at 1925 keV, where both proton and neutron configurations have a non-negligible role, is dependent on both e^p and e^n. Although this $B(E3)$ value comes out to be much less and no γ decay of $\Delta J = 3$ in nature is known from this 1925-keV level, nonetheless, the present calculation and comparison clearly indicate the difference in contribution of the proton and neutron in the structure of the first two $11/2^-$ levels in ^{131}I.

Among the $11/2^-$ levels in the neighboring iodine nuclei shown in Fig. 7, the level lifetimes or their limits are known in the case of ^{121}I, ^{123}I, and ^{125}I. Although pure $E1$ is known only for ^{123}I, the $B(E1)$ strengths known for the $11/2^- \rightarrow 9/2^+$ decays for all these cases are $1.65(21) \times 10^{-5}$ W.u. (^{121}I), $6(3) \times 10^{-5}$ W.u., $3.3(17) \times 10^{-6}$ W.u. (^{123}I), and $>2.3 \times 10^{-5}$ W.u. (^{125}I), respectively [26]. No $E3$ decay is known for these levels and it was not possible to compare $B(E3)$ strengths for the $11/2^-$ levels in the lighter iodine nuclei to that obtained for ^{131}I.

TABLE III. The $B(E1)$ and $B(E3)$ transition strengths for the decay of negative parity levels in ^{131}I.

E_i (keV)	J_i	E_f (keV)	J_f	E_γ (keV)	Multipole (λ)	$B(E\lambda)$ W.u.		
						expt.	NUSHELLX	
							$e^p = 3.0$	$e^p = 2.0$
1646	$11/2^-$	852	$9/2^+$	794	$(E1)$	$2.6(8) \times 10^{-5}$		
		1060	$9/2^+$	586	$(E1)$	$1.0(3) \times 10^{-5}$		
		150	$5/2^+$	1496	$(E3)$	<14	11	5.5
1797	$15/2^-$	1556	$15/2^+$	241	$E1$	$1.6(2) \times 10^{-6}$		
		1596	$13/2^+$	201	$E1$	$2.8(3) \times 10^{-6}$		
1899	$13/2^-$	774	$11/2^+$	1126	$(E1)$	$4.3(1.0) \times 10^{-6}$		

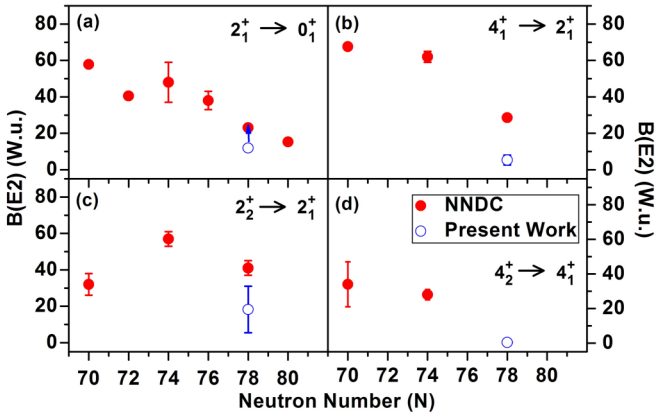

FIG. 9. The $B(E2)$ values for the decays of ^{132}Xe levels in comparison to that in neighboring nuclei. The filled circles represents the values calculated from the level lifetimes taken from NNDC database [26]. The open circle is for ^{132}Xe and are measured in the present work. The branching and mixing ratios are taken from NNDC database.

B. ^{132}Xe

The even-even Xe isotopes are known to have a transitional behavior from γ soft to vibrational, as one moves towards the $N = 82$ shell closure [43,44]. The $E_{4_1^+}/E_{2_1^+}$ ratio for ^{132}Xe comes out to be 2.16 which indicates a vibrational structure for this nucleus. From our present shell model calculation also, this ratio comes out to be 2.06 which is in good agreement with the experimental one. Very good agreement of experimental data and present calculation was also found for all other yrast levels in this nucleus. This indicates that the present calculation could nicely reproduce the structure of the collective low-lying levels in ^{132}Xe. The approach towards the vibrational nature for the Xe nuclei are also indicated in the very recent work by Kaya *et al.* [45] where shell model calculations with $sn100pn$ interaction was also performed. The present calculation was found to reproduce those results obtained for ^{132}Xe in full valence space by Kaya *et al.* However, in the present shell model calculation, the 3_1^+ level is predicted at a higher excitation compared to 4_2^+; also the 2_3^+ level is predicted at a lower excitation compared to both the 4_2^+ and 3_1^+ levels. The earlier shell model calculation with $sn100pn$ interaction made similar predictions on the 3_1^+ level [12] and none of the previous calculations [12,31] showed the excitation energy of the 2_3^+ level which is, however, identified as a mixed symmetry state in Ref. [46]. The level at 1850 keV is shown as 0^+ and 2^+ in NNDC [22]. However, our calculation predicts a 0^+ level at 1697 keV, indicating that the level at 1850 keV might be a 0^+.

The collective nature of the low-lying levels in ^{132}Xe is also indicated from the strong configuration mixing observed for these levels as discussed in Sec. IV. In fact, almost ∼45% of the partitions have strength <1% for the 0^+ levels and this increases to almost 70% for other levels (2^+, 3^+, and 4^+) in ^{132}Xe.

Figure 9 shows the reduced $E2$ transition probabilities for the decay of a few low lying levels in Xe nuclei as a function of neutron number up to the shell closure at $N = 82$. The lifetime data obtained in the present work add the points at $N = 78$ for the 2_1^+, 4_1^+, 2_2^+, and 4_2^+ levels. The absolute $B(E2)$ values for these levels supports their collective nature and the decrease in $B(E2)$ values for all these low-lying levels conjectures the validity of double shell closure at ^{132}Sn.

VI. SUMMARY

The lifetimes of a few low-lying excited levels in ^{131}I and ^{132}Xe have been measured by using a γ-γ fast timing technique with the generalized centroid difference method and VENTURE array. A large basis shell model calculation was performed using NUSHELLX code that could well explain the excitation energies and level lifetimes of the low-lying excited levels in ^{131}I and ^{132}Xe. The strong configuration mixing observed from the calculation represents the collective nature of these levels which is also supported from the energy ratios and $B(E2)$ strengths. The decrease in $B(E2)$ values with increase in neutron number up to $N = 82$, both in ^{131}I and ^{132}Xe, supports the validity of double shell closure of ^{132}Sn. The $E1$ decays of the negative parity levels in ^{131}I are compared with the systematics of similar decay patterns in the neighboring isotopes. The possibility of octupole excitation in the structure of these levels is discussed based on the $B(E1)$ and $B(E3)$ rates and these were found to be enhanced for the 1646 keV, $11/2^-$ level in ^{131}I.

ACKNOWLEDGMENTS

The effort of the staf and members of the K-130 cyclotron operation group at VECC, Kolkata, is gratefully acknowledged for providing a high quality alpha beam. S.S.A. would like to acknowledge the support from BRNS (Sanction No. 2013/38/02-BRNS/1927 for PRF, BRNS, dated 16 October 2013) towards his Ph.D. fellowship. The efforts of R. K. Chatterjee, RCD, VECC is acknowledged for his assistance in target preparation and radio-chemical separation. A.S. acknowledges the UGC JRF/SRF fellowship [Ref. No 17-06/2012(i)EU- V] in support of participation in the present work. A. Choudhury and S. Imran, VECC, are acknowledged for their effort towards daily maintenance of the clover detectors during experiment.

[1] P. Bhattacharyya, P. J. Daly, C. T. Zhang, Z. W. Grabowski, S. K. Saha, R. Broda, B. Fornal, I. Ahmad, D. Seweryniak, I. Wiedenhover, M. P. Carpenter, R. V. F. Janssens, T. L. Khoo, T. Lauritsen, C. J. Lister, P. Reiter, and J. Blomqvist, Phys. Rev. Lett. **87**, 062502 (2001).

[2] P. Bhattacharyya, P. J. Daly, C. T. Zhang, Z. W. Grabowski, S. K. Saha, B. Fornal, R. Broda, W. Urban, I. Ahmad, D. Seweryniak, I. Wiedenhover, M. P. Carpenter, R. V. F. Janssens, T. L. Khoo, T. Lauritsen, C. J. Lister, P. Reiter, and J. Blomqvist, Phys. Rev. C **64**, 054312 (2001).

[3] R. A. Meyer *et al.*, Phys. Rev. C **13**, 1617 (1976).
[4] C. A. Stone, S. H. Faller, and W. B. Walters, Phys. Rev. C **39**, 1963 (1989).
[5] J. M. Allmond, A. E. Stuchbery, J. R. Beene, A. Galindo-Uribarri, J. F. Liang, E. Padilla-Rodal, D. C. Radford, R. L. Varner, A. Ayres, J. C. Batchelder, A. Bey, C. R. Bingham, M. E. Howard, K. L. Jones, B. Manning, P. E. Mueller, C. D. Nesaraja, S. D. Pain, W. A. Peters, A. Ratkiewicz *et al.*, Phys. Rev. Lett. **112**, 172701 (2014).
[6] H. Mach, D. Jerrestam, B. Fogelberg, M. Hellström, J. P. Omtvedt, K. I. Erokhina, and V. I. Isakov, Phys. Rev. C **51**, 500 (1995).
[7] S. H. Liu, J. H. Hamilton, A. V. Ramayya, J. K. Hwang, A. V. Daniel, G. M. Ter-Akopian, Y. X. Luo, J. O. Rasmussen, S. J. Zhu, and W. C. Ma, Phys. Rev. C **79**, 067303 (2009).
[8] P. Hoff, P. Baumann, A. Huck, A. Knipper, G. Walter, G. Marguier, B. Fogelberg, A. Lindroth, H. Mach, M. Sanchez-Vega, R. B. E. Taylor, P. VanDuppen, A. Jokinen, M. Lindroos, M. Ramdhane, W. Kurcewicz, B. Jonson, G. Nyman, Y. Jading, K.-L. Kratz *et al.* (ISOLDE Collaboration), Phys. Rev. Lett. **77**, 1020 (1996).
[9] B. Fogelberg, M. Hellstrom, D. Jerrestam, H. Mach, J. Blomqvist, A. Kerek, L. O. Norlin, and J. P. Omtvedt, Phys. Rev. Lett. **73**, 2413 (1994).
[10] J. P. Omtvedt, H. Mach, B. Fogelberg, D. Jerrestam, M. Hellstrom, L. Spanier, K. I. Erokhina, and V. I. Isakov, Phys. Rev. Lett. **75**, 3090 (1995).
[11] S. Ilieva, T. Kroll, J. M. Regis, N. Saed-Samii, A. Blanc, A. M. Bruce, L. M. Fraile, G. deFrance, A. L. Hartig, C. Henrich, A. Ignatov, M. Jentschel, J. Jolie, W. Korten, U. Koster, S. Lalkovski, R. Lozeva, H. Mach, N. Marginean, P. Mutti *et al.*, Phys. Rev. C **94**, 034302 (2016).
[12] A. Vogt *et al.*, Phys. Rev. C **96**, 024321 (2017).
[13] W. F. Mueller, M. P. Carpenter, J. A. Church, D. C. Dinca, A. Gade, T. Glasmacher, D. T. Henderson, Z. Hu, R. V. F. Janssens, A. F. Lisetskiy, C. J. Lister, E. F. Moore, T. O. Pennington, B. C. Perry, I. Wiedenhover, K. L. Yurkewicz, V. G. Zelevinsky, and H. Zwahlen, Phys. Rev. C **73**, 014316 (2006).
[14] K. Selvakumar, A. K. Singh, C. Ghosh, P. Singh, A. Goswami, R. Raut, A. Mukherjee, U. Datta, P. Datta, S. Roy, G. Gangopadhyay, S. Bhowal, S. Muralithar, R. Kumar, R. P. Singh, and M. K. Raju, Phys. Rev. C **92**, 064307 (2015).
[15] P. Mason *et al.*, Phys. Rev. C **72**, 064315 (2005).
[16] J. M. Règis *et al.*, Nucl. Instrum. Methods Phys. Res., Sect. A **823**, 72 (2016).
[17] S. S. Alam *et al.*, Nucl. Instrum. Methods Phys. Res., Sect. A **874**, 103 (2017).
[18] B. A. Brown and W. D. M. Rae, Nucl. Data Sheets **120**, 115 (2014).
[19] A. Saha *et al.*, Nucl. Phys. A **976**, 1 (2018) and reference therein.
[20] G. Jakob, N. Benczer-Koller, G. Kumbartzki, J. Holden, T. J. Mertzimekis, K.-H. Speidel, R. Ernst, A. E. Stuchbery, A. Pakou, P. Maier-Komor, A. Macchiavelli, M. McMahan, L. Phair, and I. Y. Lee, Phys. Rev. C **65**, 024316 (2002).
[21] Yu. Khazov, I. Mitropolsky, and A. Rodionov, Nucl. Data Sheets **107**, 2715 (2006).
[22] Yu. Khazov *et al.*, Nucl. Data Sheets **104**, 497 (2005).
[23] O. Naviliat-Cuncic *et al.*, Nucl. Instrum. Methods Phys. Res., Sect. A **287**, 487 (1990).
[24] S. Raman, C. W. Nestor, Jr., and P. Tikkanen, At. Data Nucl. Data Tables **78**, 1 (2001).
[25] J. M. Régis, J. Jolie, N. Saed-Samii, N. Warr, M. Pfeiffer, A. Blanc, M. Jentschel, U. Koster, P. Mutti, T. Soldner, G. S. Simpson, F. Drouet, A. Vancraeyenest, G. deFrance, E. Clement, O. Stezowski, C. A. Ur, W. Urban, P. H. Regan, Z. Podolyak *et al.*, Phys. Rev. C **95**, 054319 (2017).
[26] www.nndc.bnl.gov/ensdf/.
[27] B. A. Brown, N. J. Stone, J. R. Stone, I. S. Towner, and M. Hjorth-Jensen, Phys. Rev. C **71**, 044317 (2005).
[28] R. Machleidt, F. Sammarruca, and Y. Song, Phys. Rev. C **53**, R1483 (1996).
[29] T. Kibdi *et al.*, Nucl. Instrum. Methods Phys. Res., Sect. A **589**, 202 (2008).
[30] H. Morinaga and T. Yamazaki, *In-beam Gamma-ray Spectroscopy* (North-Holland, New York, 1976), p. 68.
[31] E. Teruya, N. Yoshinaga, K. Higashiyama, and A. Odahara, Phys. Rev. C **92**, 034320 (2015).
[32] G. Lhersonneau *et al.*, Phys. Rev. C **12**, 609 (1975).
[33] H. Watanabe, G. J. Lane, G. D. Dracoulis, A. P. Byrne, P. Nieminen, F. G. Kondev, K. Ogawa, M. P. Carpenter, R. V. F. Janssens, T. Lauritsen, D. Seweryniak, S. Zhu, and P. Chowdhury, Phys. Rev. C **79**, 064311 (2009).
[34] E. S. Macias and W. B. Walters, Nucl. Phys. A **161**, 471 (1971).
[35] S. H. Devare, R. M. Singru, and H. G. Devare, Phys. Rev. **140**, B536 (1965).
[36] L. M. Beyer and W. H. Kelly, Nucl. Phys. A **104**, 274 (1967).
[37] S. Biswas, R. Palit, A. Navin, M. Rejmund, A. Bisoi, M. S. Sarkar, S. Sarkar, S. Bhattacharyya, D. C. Biswas, M. Caamano, M. P. Carpenter, D. Choudhury, E. Clement, L. S. Danu, O. Delaune, F. Farget, G. deFrance, S. S. Hota, B. Jacquot, A. Lemasson *et al.*, Phys. Rev. C **93**, 034324 (2016).
[38] G. de Angelis *et al.*, Phys. Lett. B **535**, 93 (2002).
[39] S. M. Burnett *et al.*, Nucl. Phys. A **432**, 514 (1985).
[40] R. H. Spear, At. Data Nucl. Data Tables **42**, 55 (1989).
[41] B. Bucher, S. Zhu, C. Y. Wu, R. V. F. Janssens, D. Cline, A. B. Hayes, M. Albers, A. D. Ayangeakaa, P. A. Butler, C. M. Campbell, M. P. Carpenter, C. J. Chiara, J. A. Clark, H. L. Crawford, M. Cromaz, H. M. David, C. Dickerson, E. T. Gregor, J. Harker, C. R. Hoffman *et al.*, Phys. Rev. Lett. **116**, 112503 (2016).
[42] S. Sarkar and M. Saha Sarkar, Phys. Rev. C **64**, 014312 (2001).
[43] K. Nomura, R. Rodríguez-Guzman, and L. M. Robledo, Phys. Rev. C **96**, 064316 (2017).
[44] G. Puddu, O. Scholten, and T. Otsuka, Nucl. Phys. A **348**, 109 (1980).
[45] L. Kaya *et al.*, Phys. Rev. C **98**, 014309 (2018).
[46] L. Coquard, N. Pietralla, G. Rainovski, T. Ahn, L. Bettermann, M. P. Carpenter, R. V. F. Janssens, J. Leske, C. J. Lister, O. Möller, W. Rother, V. Werner, and S. Zhu, Phys. Rev. C **82**, 024317 (2010).